DEPARTMENT OF DEFENSE
VIRTUAL CORROSION CONFERENCE 2013

DoD 2013-3691

The Effect of Applied Polarization on Stress Corrosion Cracking in Sensitized AA5083

Cortney B. Crane
Department of Materials Science and Engineering
University of Virginia
Charlottesville, VA 22904
USA

Richard P. Gangloff
Department of Materials Science and Engineering
University of Virginia
Charlottesville, VA 22904
USA

ABSTRACT

Marine structures fabricated from non-heat treatable Al-Mg alloys may become susceptible to intergranular corrosion (IGC) and intergranular stress corrosion cracking (IGSCC) due to in-service grain boundary β (Al_3Mg_2) precipitation; a process known as sensitization. The hypothesized coupled β-dissolution and crack tip hydrogen embrittlement mechanism for IGSCC in sensitized Al-Mg alloys provides a fundamental basis for management of such damage in ship structures. Experiments validate this mechanism. Fracture mechanics-based slow-rising displacement experiments establish the dominant role of bulk-applied potential in affecting rates of both IGC and IGSCC for laboratory sensitized AA5083-H131 (100 ^{o}C for 175 h, nitric acid mass loss of 22 mg/cm^2) in the susceptible S-L orientation. Applied anodic potential (-0.730 V_{SCE}) causes increased crack growth rate by enhanced β and Al-Mg solid solution dissolution for crack acidification through Al^{+3} and Mg^{+2} hydrolysis leading to substantial crack tip atomic hydrogen production/uptake. In contrast cathodic polarization precludes crack acidification and damaging H uptake provided that polarization is maintained below both the matrix and β-breakdown potentials. Intergranular SCC was nearly eliminated for this susceptible crack orientation of sensitized AA5083 at applied potentials below -1.020 V_{SCE} to -1.080 V_{SCE}. A crack tip mechanics model based on H diffusion limitation of IGSCC growth rate exists to couple with crack tip fracture process zone H concentration, and suggests a sub-micrometer critical distance. Controlled cathodic polarization could mitigate IGC and IGSCC in sensitized Al-Mg alloy components.

Key words: AA5083, IGSCC, polarization, hydrogen embrittlement

INTRODUCTION

Non-heat treatable Al-Mg alloys are used as steel substitutes for modern naval structures due to their combined high strength to weight ratio, weldability and general corrosion resistance. These alloys are solid solution strengthened with Mg; however, when the Mg concentration exceeds 3 wt. pct. the alloy may be susceptible to intergranular corrosion (IGC) and intergranular stress corrosion cracking (IGSCC) in neutral chloride solutions due to sensitization.[1] Sensitization occurs when the reactive anodic β phase

(Al_3Mg_2) precipitates on grain boundaries during extended exposure at 40-180 °C, and provides a preferred-intergranular path for localized IGC and IGSCC.[2–6] Few studies probed the dependencies of IGC and IGSCC on the degree of low temperature sensitization (below 125 °C); reported crack growth kinetics were not sufficiently quantified to either test proposed mechanisms of IGSCC or to enable engineering decisions regarding component fitness-for-mission.[1,7–10]

An extension of recent work[11] broadly characterized the IGSCC susceptibility of alloy AA5083-H131 stressed in near-neutral NaCl solution and these results are summarized in Figure 1.[12] Crack growth rates were measured as a function of rising stress intensity (K) during slow displacement rate loading of a fatigue precracked specimen in the susceptible S-L orientation (stress parallel to the plate thickness (S) and crack growth in the plate-rolling direction (L)). Applied potential was fixed at -0.800 $V_{SCE,}$ which is in the range of open circuit potential (OCP) of AA5083 in NaCl (OCP typically falls from -0.750 V_{SCE} to -0.900 V_{SCE} as corrosion occurs)[13]. The threshold stress intensity for the onset of IGSCC (K_{TH} in Figure 1a) and the nearly K-independent crack growth rate at a K of 15 MPa√m (da/dt_{K15} in Figure 1b) are plotted as a function of low temperature (60-100 °C) degree of sensitization (DoS) in the range of 3 mg/cm^2 to 50 mg/cm^2, as represented by coupon mass loss per ASTM International Standard G67.[14] Several features are notable in Figure 1, including: (a) the very low K_{TH} and high da/dt_{K15} for DoS in excess of about 15 mg/cm^2, demonstrating severe IGSCC, and (b) the existence of a critical DoS, near 10 mg/cm^2, below which IGSCC is minimal to nil and near the resolution limit (0.5 nm/s to 1 nm/s) for da/dt measurement. This resolution limit is based on growth measured in air, which can be attributed to low level hydrogen environment assisted cracking (HEAC) in moist air, creep crack growth, or false growth due to plasticity from rising K.[15] The low level crack growth measured for AA5083-H131 with DoS below 10 mg/cm^2 and stressed in NaCl at -0.800 V_{SCE} may be attributed to these factors. Slow rate IGSCC cannot be ruled out. Fractography of as-received specimens in NaCl showed discrete intergranular cracking close to the fatigue precrack, demonstrating that low level IGSCC can and did occur in this resistant microstructure.

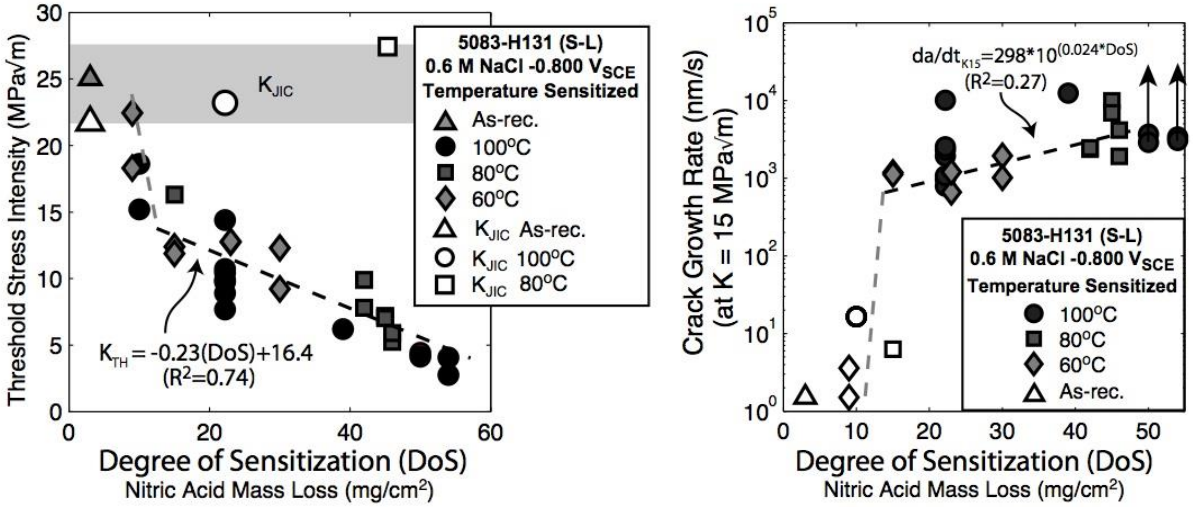

Figure 1: The a) threshold stress intensity, K_{TH}, and b) Stage II crack growth rate at K=15 MPa√m, da/dt_{K15}, for AA5083-H131 (S-L and initial dK/dt = 0.25 MPa√m/h) in NaCl at -0.800 V_{SCE} as a function of laboratory sensitization at 60 °C, 80 °C and 100 °C for various times.[12] Degree of sensitization is measured with the ASTM G67 nitric acid mass loss test.[14,22] The range of fracture toughness (K_{JIC} from J-integral analysis) is shown by the grey bar in a).[12] Open data points in b) represent da/dt where K_J of 15 MPa√m is in Stage I or earlier.

The experiments represented in Figure 1 also demonstrated that the fatigue precrack extended by corrosion during prolonged exposure to this environment at a low K level below the classic K_{TH}.[12] This behavior was ascribed to IGC promoted within the occluded fatigue crack, perhaps associated with applied stress, and depended on DoS for the conditions shown in Figure 1. This behavior demonstrates the potential severity of crack advance at very low stress intensity levels and this measurement provides an alternative to boldly exposed surface measurements of IGC rates using quantitative microscopy. Parallel research is investigating IGC in AA5083-H131, and the results are relevant to understanding the mechanism(s) for the IGSCC behavior characterized in Figure 1.[13,16–21]

The hypothesized mechanism for IGSCC in sensitized Al-Mg alloys is coupled β precipitate dissolution, solid solution Al-Mg matrix (α) dissolution, and atomic hydrogen (H) production/uptake at the occluded crack tip causing HEAC.[7,11,12,23,24] Crack growth in near-neutral NaCl begins with limited dissolution of the passive Al-4%Mg matrix, which leads to mild hydrolytic acidification at near OCP. In parallel grain boundary β dissolution provides critical promotion of high concentrations of Al^{+3} and Mg^{+2} in the crack solution, which facilitates α breakdown. Specifically, hydrolysis of the concentrated Al^{+3} and Mg^{+2} solution enables near equilibrium acidification (pH 2-3) compared to that possible (pH 5) from weak Al^{+3} hydrolysis alone. Lowered pH increases crack tip overpotential for H production and subsequent uptake. This high concentration of H diffuses into the fracture process zone (FPZ) and, with locally concentrated tensile stress, promotes inter-β ligament H embrittlement along the grain boundary. There are two implications associated with this proposed mechanism. First, the very rapid da/dt levels shown in Figure 1 may not be sustainable by H diffusion in the crack tip process zone.[25] However, recent analysis demonstrated that H diffusion is capable of sustaining crack growth rates on the order of 100 μm/s provided that such transport is not hindered by H trapping and crack tip surface H solubility is high.[23] A proposed precipitate and dislocation free zone proximate to dissolved and intact β could provide a situation for minimal H trapping and hence rapid H diffusion.[23] Second, the proposed mechanism suggests that IGSCC can be greatly reduced if the critical step of dissolution/breakdown of anodically reactive β is stifled so that H production and uptake are reduced to levels typical of a mildly acidic crack tip. Cathodic polarization provides a practical means to eliminate β breakdown, and literature results suggest that IGSCC is mitigated by this approach.[1,7,26] However, detailed experimental data are necessary to establish the beneficial effect of cathodic polarization, particularly given the lack of such crack growth rate data for sensitized Al-Mg alloys, as well as the possibility for both localized crack tip hydrogen embrittlement and severe-alkaline corrosion.

The objective of this work is to experimentally characterize the effect of applied potential on the kinetics of IGSCC in sensitized Al-Mg, building on the results shown in Figure 1 and specifically aimed at validating the hypothesized crack tip β-α dissolution and H embrittlement mechanism. Crack growth experiments focus on the susceptible S-L orientation of sensitized AA5083-H131 stressed in NaCl solution at various-constant bulk potentials. This susceptible orientation isolates the effect of crack tip electrochemistry on da/dt, apart from the complicating role of a tortuous intergranular crack path through the microstructure. Moreover, such growth rates are relevant to fracture mechanics simulation of mixed mode cracking in anisotropic-sensitized plate under complex bending.[9] Crack growth rate results are interpreted in the context of occluded-crack mass transport and electrochemical reaction kinetics which establish crack tip pH, potential and H overpotential that drives HEAC.[15] The experimental results presented in this paper provide a basis to consider the practical benefit of cathodic potential control as a route to manage IGC and IGSCC in sensitized Al-Mg components in the marine environment.

EXPERIMENTAL PROCEDURE

Subcritical crack growth experiments were performed on a partially recrystallized 5.7 cm thick plate of AA5083-H131 (Al-4.4Mg-0.7Mn-0.08Cr, wt. pct.)[27], with reported tensile yield strength (σ_{YS}, 335 MPa) and ultimate tensile strength (σ_{UTS}, 353 MPa), both in the L direction.[27] Measured-compressive yield strength of as-received plate (DoS of 3 mg/cm^2) was 258 MPa. Plane strain fracture toughness, K_{JIC}, of 21.7 MPa$\sqrt{m}$ (as-received, DoS of 3 mg/cm^2) was measured for the S-L orientation using an elastic-

plastic J-integral method.[12] The grain structure was highly anisotropic throughout the mid-75% of the plate where IGSCC was studied.

Following laboratory sensitization at 100°C for 175 h (DoS = 22 mg/cm^2, compressive yield strength = 263 MPa, K_{JIC} = 23.2 MPa$\sqrt{m}$), single edge notch tensile (SENT) specimens were machined in the S-L orientation with a notch depth of 1.5 mm, width of 17.3 mm and thickness of 6.6 mm.[12] These specimens were fatigue precracked in moist air to a notch plus fatigue crack depth of 3.3 mm and final-maximum K of 3.5 MPa$\sqrt{m}$. The SENT specimen was fully immersed in NaCl contained in a 185 mL Plexiglas cell. Solution was circulated through the cell at 30 mL/min from a 2 L reservoir at ambient temperature. The specimen was loaded in solution under constant grip displacement rate control to a K of 4 MPa$\sqrt{m}$ and held at constant load for 10 h. Immediately following this hold, the specimen was loaded at an initial rate (dK/dt) of 0.25 MPa$\sqrt{m}$/h to the onset of stable crack growth where both K and dK/dt increased until final fracture. Open circuit potential and pH were monitored before and after each experiment. An ungrounded Wenking potentiostat (model LB 81M) maintained a fixed potential on a grounded SENT specimen during loading for experiments ranging from -0.730 V_{SCE} to -1.300 V_{SCE}.

A computer-automated direct current potential difference (dcPD) method was used to continuously measure crack length, *a*.[28,29] False growth due to current supply variation, as well as temperature and uniform-strain-based resistance and resistivity changes, were mitigated by using reference probes on all specimens.[28,29] Crack growth rate, da/dt, was calculated at a given time, *t*, with a second-order polynomial fit to *a* versus *t* over *t* ± 3 or ± 10 data points. Experiments in air or with IGSCC resistant potentials were analyzed with elastic-plastic stress intensity, K_J, determined by J-integral analysis.[12]

RESULTS AND DISCUSSION

The results of this research provide two contributions. First, the proposed mechanism for IGSCC of sensitized Al-Mg alloys is validated; that is, β-α dissolution generates the critical chemistry for crack tip H production and uptake required for H embrittlement of Al grain boundaries. Specific results demonstrate that β dissolution is uniquely necessary for IGSCC in Al-Mg alloys. The data in Figure 1 show that as-received AA5083-H131 resists IGSCC in 0.6 M NaCl when polarized to near OCP, because β is not present at grain boundaries. When grain boundary β precipitates are discontinuously present, from low temperature sensitization producing a DoS of 10 mg/cm^2 and higher, AA5083-H131 becomes highly susceptible to IGSCC at this near-OCP potential, establishing the requirement of grain boundary β presence. An IGC and IGSCC susceptible sensitized microstructure of Al-Mg (specifically 22 mg/cm^2) resists IGC and IGSCC when cathodically polarized in NaCl solution. The da/dt is reduced to the resolution limit of the crack growth measurement system when fatigue precracked specimens are polarized below the breakdown potential of β, which strongly reduces dissolution of both α and β.[15] The combination of these results validate the hypothesis that β dissolution is necessary to trigger the critical crack tip chemistry for significant α dissolution leading to H production/uptake and H embrittlement of Al grain boundaries in the time frame of the rising-K experiments. The experimental approach provides the first reported measurement of the rate of low K IGC ahead of an occluded fatigue crack tip in sensitized Al-Mg. Low K IGC rates can be compared to rates of IGC which are measured from metallographic sections of localized corrosion growth from a boldly exposed surface without stress. Collectively, these measurements of IGC provide the kinetics for corrosion growth modeling in components and for assessment of electrochemical understanding of localized corrosion along sensitized grain boundaries in Al-Mg.[11–13,16] Such electrochemical considerations pertinent to IGC provide a basis for understanding the effect of applied potential on occluded crack chemistry, which in turn controls rates of IGSCC, as considered in the following sections

IGC-fissure tip electrochemistry developed as a function of potential

The rate of IGC, progressing from a fatigue precrack in sensitized AA5083 in near-neutral 0.6 M NaCl, depends on applied potential. Extension of IGC during the low static-K hold for 10 h, then the initial-slow-

rising K segment of the SENT experiment, is shown in Figure 2. The nature of applied polarization is relative to the initial-measured OCP of about -0.760 V_{SCE}, which is expected to decrease to about -0.900 V_{SCE} as corrosion occurs.[13] With anodic polarization at -0.730 V_{SCE}, extremely rapid IGC commenced with minimal incubation time and was sensibly constant (da/dt of 8.4 nm/s) during the 10 h hold at 4 MPa√m. A 4-fold drop in IGC rate to an average of 1.4 nm/s (between 0.80 nm/s and 2.6 nm/s) was observed for extensive-replicate experiments polarized to -0.800 V_{SCE}.[12] Average growth rate during the hold period continued to decrease with polarization to -0.900 V_{SCE} and -0.975 V_{SCE} (0.9 nm/s and 0.4 nm/s, respectively). A second drop of over 10 times (0.4 nm/s to 0.03 nm/s) is seen between -0.975 V_{SCE} and -1.020 V_{SCE}. At further cathodic potentials (-1.080 V_{SCE}, -1.100 V_{SCE}, and -1.300 V_{SCE}) rates remain at this low level, then begin to increase (0.05 nm/s, 0.05 nm/s, 0.31 nm/s respectively). These low rates are somewhat faster than the system resolution limit represented by false crack growth measured in air at 4 MPa√m (0.004 nm/s). For each potential below -0.900 V_{SCE}, growth rate accelerated after the constant K hold transitioned to the slow-rising K up to 6 MPa√m. The result measured at an applied potential of -0.975 V_{SCE} did not exhibit this acceleration. This anomaly may be due to a malfunctioning potentiostat, which caused corrosion prior to the initiation of the test and caused the OCP at the onset of loading to equal -0.900 V_{SCE}.

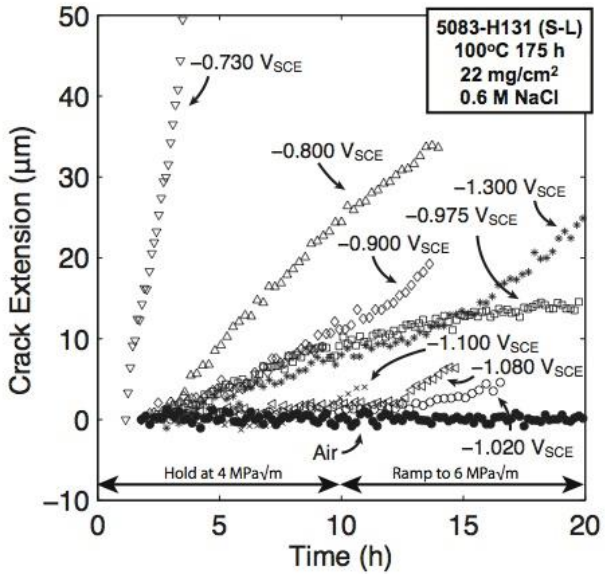

Figure 2: Crack extension versus time for AA5083-H131 (S-L) sensitized at 100 °C for 175 h (22 mg/cm²), immersed in 0.6 M NaCl and held at 4 MPa√m, then loaded at 0.25 MPa√m/h to 6 MPa√m for various constant-applied potentials.

All growth rates measured during the constant-K hold period are plotted as a function of bulk-applied potential in Figure 3. The breakdown potential of α ($E_{Br-\alpha}$ of -0.870 V_{SCE}) in acidic (-0.8 pH) simulated crack tip solution[19,20], and the range of environment sensitive breakdown potentials of β ($E_{Br-\beta}$ of -0.960 V_{SCE} in 0.6 M NaCl[31] and -1.015 V_{SCE} in acidic simulated crack tip solution[19,20]) are plotted for reference. The breakdown potential for the Al-4%Mg solid solution in neutral 0.6 M NaCl was not reported, however the breakdown potential for Al-0.9%Mg in deaerated 0.1 M NaCl was reported as -0.680 V_{SCE} and decreases with increasing Mg content.[32] Therefore the range of $E_{Br-\alpha}$ could be between -0.680 V_{SCE} (or somewhat higher) and -0.870 V_{SCE} depending on pH of the environment. All breakdown potentials were measured from potentiodynamic scans and are therefore specific to the scan rate, associated corrosion history, and definition of E_{Br}.[19–21,32]

The highest value of da/dt shown in Figure 3 (8.4 nm/s at -0.730 V_{SCE}) is of the same order of magnitude as the growth rate (2.1 nm/s) from a metallographic sectioning study of IGC extending from an unstressed boldly exposed surface of the same lot and sensitization condition of AA5083-H131.[22] This metallographic rate includes both initiation and propagation of IGC, and therefore is expected to be somewhat slower than fatigue precrack corrosion extension where continuous dcPD measurement of corrosion growth

provides accurate-average rates. The strong-beneficial effect of decreasing-applied potential on IGC rate (bold surface, unstressed) was predicted for sensitized Al-Mg in 0.6 M NaCl.[19,20] Rates were modeled with Faraday's Law using a series formulation of phase-fraction weighted current densities measured from potentiodynamic scans of α and β in acidic simulated fissure solution.[19,20] Modeled rates are on the same order of magnitude, but are consistently slower than those measured using fatigue precracked specimens (Figure 3). When fatigue precracked and sensitized AA5083-H131 in near neutral NaCl is polarized well above the β breakdown potential, β dissolution dominates to produce Al^{+3} and Mg^{+2} which hydrolyze to generate an acidic fissure tip. This acidification triggers dissolution of α by lowering $E_{Br-\alpha}$ to -0.870 V_{SCE}. Above this potential, dissolution of both α and β sustains an equilibrium acidic fissure tip at pH 2-3 and ensuing rapid IGC growth.[12,15]

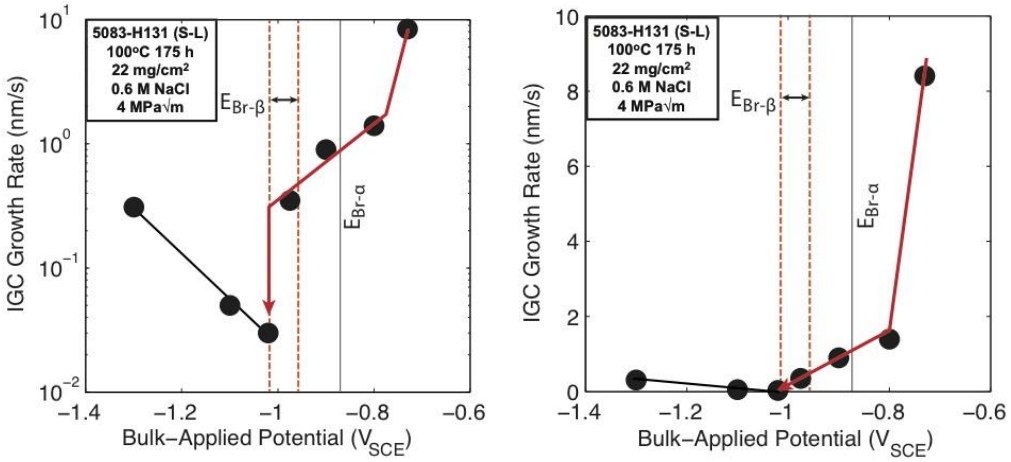

Figure 3: Rates of fatigue crack IGC on a: a) logarithmic and b) linear scale for sensitized AA5083-H131 (S-L, 22 mg/cm²) during a hold at 4 MPa√m. The breakdown potential of α in simulated crack tip solution is shown with the thin vertical line, and the range of pH-sensitive β breakdown potentials is shown by dashed lines.

The modeled bold-surface IGC rates[19,20] exhibited two strong drops with declining applied potential, consistent with the data in Figure 3. The predicted decrease at the higher potential (-0.850 V_{SCE}) coincides with the dramatic decrease in the anodic current density as applied potential falls below the breakdown potential for rapid α dissolution in acidic solution ($E_{Br-\alpha}$= -0.870 V_{SCE}).[19,20] The first strong change in the rate of IGC at the fatigue crack tip, between -0.800 V_{SCE} and -0.760 V_{SCE}, also coincides with the $E_{Br-\alpha}$ = -0.870 V_{SCE} (This sharp decrease is particularly apparent in Figure 3b, which is plotted in terms of linear da/dt versus linear applied potential). The drop in Figure 3 occurs at potentials slightly positive above $E_{Br-\alpha}$ and may be accounted for by IR drop at the occluded fatigue crack-fissure tip. For example, when the bulk-applied potential for the cracked specimen was held at -0.800 V_{SCE} (anodic to the current OCP), the resistance within the occluded fatigue crack cathodically polarizes the tip potential towards a limit given by the local OCP, which in an acidic tip is close to -0.900 V_{SCE}. With IR correction, the fatigue crack tip could be below $E_{Br-\alpha}$ in the acidic environment, consistent with the importance of $E_{Br-\alpha}$. An effect of crack tip IR does not explain why the crack tip rates in Figure 3 are 4 times faster than the unstressed modeled rates,[19,20] which do not include corrosion initiation time and are therefore comparable to the dcPD-based measurement of da/dt for IGC. The source of this difference is not understood, but could be due to an effect of fatigue crack tip stress or plastic strain even at very low K. Such a stress effect is further suggested by the mild-K dependence of IGC rate during initial constant displacement rate loading (Figure 4).[12] While the possibility of a stress effect on IGC must be further examined, this effect should not be confused with the dramatic rise in da/dt at K_{TH} for the more anodic levels of polarization, which suggests a fundamental change in crack tip damage mechanism due to H embrittlement. The potential dependent chemistry developed in the crack tip and role of crack tip IR difference are detailed elsewhere.[15] Notable in this interpretation, $E_{Br-\alpha}$ is likely to be above -0.680 V_{SCE} for neutral NaCl solution, as reported for Al-0.9%Mg in dearated 0.1 M NaCl.[32] In neutral NaCl without β dissolution, IGC would

not be expected for any of the potentials represented in Figure 3, as is the case for unsensitized AA5083.[15] The presence and dissolution of β is the critical element that enables the crack solution to acidify and thus reduce $E_{Br-\alpha}$ such that IGC can progress at potentials in the range of -0.800 V_{SCE}.

The decreasing IGC-da/dt values for -0.975 V_{SCE} < $E_{applied}$ < -0.800 V_{SCE} in Figure 3 likely reflect a Tafel-type decline in the dissolution rate of α and associated reduction in hydrolytic acidification likely dominated by continued β dissolution above $E_{Br-\beta}$. In this regime IGC rate continues to be controlled by the slower rate of essentially-passive α dissolution in the series configuration with discontinuously arrayed-reactive β.[12,15] This smooth decline in IGC rate is interrupted when potential falls below $E_{Br-\beta}$ of -0.960 V_{SCE} in 0.6 M NaCl[31] and -1.015 V_{SCE} in acidic simulated crack tip solution[19,20]. This sharp decrease is particularly apparent in Figure 3a, which is plotted as logarithmic da/dt_{K15} versus linear potential. The measured IGC results in Figure 3 conform to this expectation, again subject to IR consideration. Simply stated, rates of IGC are essentially 0 below the $E_{Br-\beta}$ since the crack solution will not acidify. Dissolution of either phase proceeds at a very slow rate governed by Tafel extrapolation of dissolution kinetics for a near-neutral chloride solution. The finite IGC measured for a fatigue precracked specimen polarization at -1.300 V_{SCE} (Figure 2) is likely caused by cathodic Al-Mg corrosion in the increasingly alkaline fissure tip and wake due to cathodic polarization. Details of these occluded crack and fissure environments are discussed elsewhere.[15]

IGSCC as a function of applied potential

Paralleling the dependence of IGC, applied potential strongly affects measured rates of IGSCC during slow-rising K. Crack growth rate versus K is plotted in Figure 4 for sensitized specimens of AA5083-H131 (DoS of 22 mg/cm^2) stressed in near-neutral 0.6 M NaCl at various remote polarization levels. After the low-K hold period (average IGC rates during the hold are not shown for clarity), three well defined stages of SCC are observed for each experiment polarized to -0.730 V_{SCE} and -0.800 V_{SCE}. From low to high K, the first stage represents the IGC behavior noted above. The mild K dependence below K_{TH} may be

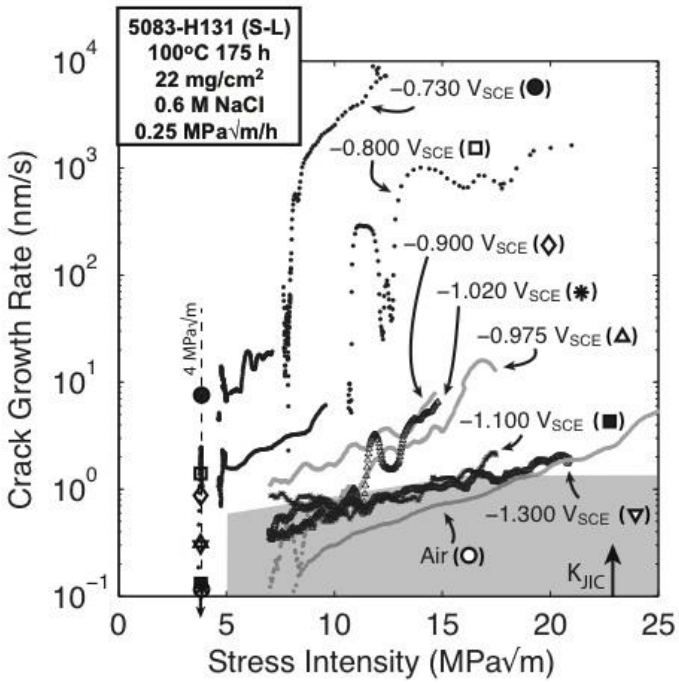

Figure 4: The K dependence of da/dt for sensitized AA5083-H131 (S-L, 22 mg/cm^2) stressed at an initial dK/dt of 0.25 MPa√m/h with various constant bulk-applied potentials. Stress intensity for specimens polarized between -1.300 V_{SCE} and -0.900 V_{SCE} and in air were determined with an elastic-plastic J-integral analysis. The grey box represents growth rate resolution for and K_{JIC} is the fracture toughness.[12]

attributed a stress sensitivity of IGC; however, a mechanism for this effect has not be reported for an actively corroding crack tip. Classic two-stage IGSCC kinetics deviate significantly from IGC kinetics at K_{TH} when polarized to both -0.730 V_{SCE} and -0.800 V_{SCE}. At -0.730 V_{SCE}, K_{TH} is 7.9 MPa√m, followed by steeply rising Stage I crack growth, leading to a reduced K dependence (Stage II) with da/dt_{II} at 15 MPa√m (da/dt_{K15}) equal to 7,200 nm/s. In seven replicate experiments at -0.800 V_{SCE}, the average K_{TH} is 10.7 MPa√m (between 8 MPa√m to 14 MPa√m), slightly K dependent da/dt in Stage II was often observed, and the average da/dt_{K15} is 3,000 nm/s (between 800 nm/s to 10,000 nm/s).[12]

Critically, crack growth rates decrease dramatically with applied potential below -0.800 V_{SCE}. For these levels of cathodic polarization and high IGSCC resistance, J-integral analysis was used to account for plasticity at higher K. For each potential, the distinction between IGC, Stage I and Stage II crack growth is obscured, and K_{TH} is not easily defined. The associated crack growth rates in Figure 4 depend on K, therefore da/dt are reported for a specific driving force (da/dt_{K15} at K=15 MPa√m) which is lower than K_{JIC}. For example at -0.900 V_{SCE}, the da/dt increase from K of 7 MPa√m to 13.5 MPa√m appears to initially follow the IGC K dependence for the -0.800 V_{SCE} case, prior to a definitive K_{TH}. The K_{TH} could be between 13 MPa√m and 15 MPa√m, but the experiment was terminated before adequate Stage I growth was produced to clearly yield a K_{TH}. For this potential, da/dt_{K15} is 8 nm/s. Similar behavior is observed for -0.975 V_{SCE} and -1.020 V_{SCE}. For -0.975 V_{SCE}, rates of IGC increase with rising K, then da/dt accelerates into Stage I defining a possible K_{TH} at about 11 MPa√m. A second acceleration occurs near 15 MPa√m, making definition of K_{TH} ambiguous; da/dt_{K15} is 4 nm/s. For -1.020 V_{SCE}, the IGC rates are slower with a strong rise at K_{TH} of 11 MPa√m and da/dt_{K15} is 6.5 nm/s. Further cathodic polarization below -1.020 V_{SCE} essentially eliminates IGSCC, as crack growth rates are only marginally above the apparent da/dt measured during loading in air when polarized to -1.080 V_{SCE}, -1.100 V_{SCE} and -1.300 V_{SCE}. These low growth rates could reflect a residual-low level of HEAC since the water vapor content of the air environment was judged to be sufficient to promote a da/dt on the order of 1 nm/s, due to H embrittlement of this slow-rising K loading.[12] Fractographic analysis was not performed to assess the extent of IGSCC, if any, for the -1.100 V_{SCE} through -1.300 V_{SCE} cases. All da/dt_{K15} are presented as a function of bulk-applied potential in Figure 5. The $E_{Br-\alpha}$ in an acidic simulated crack tip solution and the range of environment sensitive $E_{Br-\beta}$ [19,20] are plotted for reference. The K_{TH} is not plotted as a function of potential due to the ambiguity of threshold definition for the low rates of IGSCC at cathodic potentials.

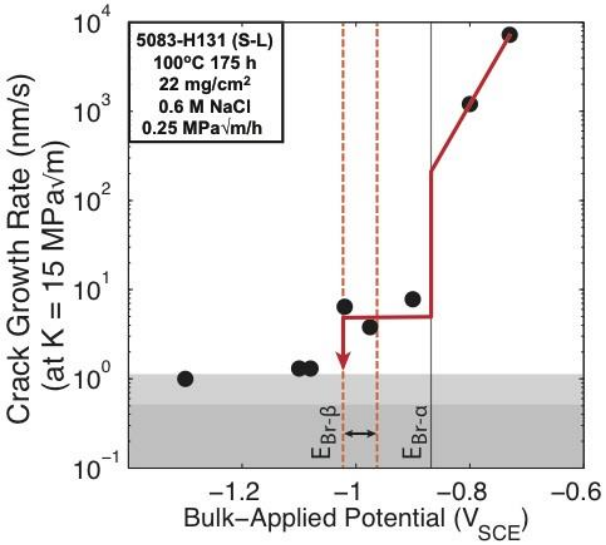

Figure 5: Crack growth rate for sensitized (DoS 22 mg/cm²) AA5083-H131 (S-L) at 15 MPa√m plotted as a function of applied potential. The breakdown potential of α in simulated crack tip solution is shown with the thin vertical line, and the range of pH-sensitive β breakdown potentials is shown by dashed lines. The resolution limit of the dcPD measurement technique is plotted as grey boxes (lower for 22 mg/cm² in air and upper for as-received 5083-H131 in air at K=15 MPa√m).

Three points are notable with regard to Figure 5. First, anodic dissolution above $E_{Br-\alpha}$ causes a severe increase in IGSCC for sensitized AA5083-H131 (S-L), due to induced α and β dissolution leading to high H production and uptake. Slow strain rate testing (SSRT) also established that anodic polarization increases IGSCC susceptibility in sensitized 5083.[1] The hypothesized mechanism indicated that IGSCC susceptibility correlated with polarization above the passive regime of β, and did not take the role of α dissolution into account.[1] Separate studies established IGSCC susceptibility during anodic polarization in essentially unsensitized 5083 stressed in near-neutral NaCl, where β dissolution is not available, through SSRT[33,34] and crack growth rate experiments with compact tension (CT) specimens [7]. For the T-L oriented crack growth at very high K (25 MPa√m) and through a recrystallized and essentially β-free microstructure of AA5083-H321 (sensitized at 175 °C for 1 h, with a DoS [35] of about 7 mg/cm^2), anodic polarization (-0.540 V_{SCE}) accelerated da/dt from 0.25 nm/s at OCP (-0.740 V_{SCE}) to 3 nm/s.[7] These da/dt levels are substantially less than the results shown in Figure 5, as expected due to the combined effects of crack orientation in the recrystallized and low DoS microstructure. None-the-less, these literature results for unsensitized AA5083 demonstrate that resistant microstructures without grain boundary β are prone to low rate IGSCC at a sufficiently anodic potential, which is likely above the $E_{Br-\alpha}$ for an initially near-neutral chloride solution. Dissolution of α alone can cause embrittlement, as long as an acidic crack tip is developed by dissolution. Use of cathodic potential and high resolution crack growth experimentation has not been reported to investigate the critical role of β in triggering α dissolution to promote H embrittlement.

Second, the lowest da/dt_{K15} values measured in NaCl at cathodic potentials, about 1 nm/s in Figure 5, are on the order of expected crack growth rates for HEAC in aluminum alloys stressed in a low-H concentration environment.[12] Moreover, plasticity-based false crack growth rates are in the range of 0.5 nm/s to 1 nm/s (grey region in Figures 4 and 5), complicating interpretation of very low rate HEAC.[12] Third, there is no evidence of an increased rate of crack growth for the highest level of cathodic polarization examined. This was confirmed for cathodic polarization (-1.390 V_{SCE}) of recrystallized AA5083-H321 (T-L) in NaCl;[7] crack growth rates remained at or below the slow level measured at OCP.[7] Conversely, tensile strength, time-to-failure, and elongation decreased during SSRT experiments on AA5083-H112 subjected to highly cathodic polarization (-1.60 V_{SCE}) in seawater.[26] This IGSCC susceptibility was attributed to H embrittlement by generation of H during overprotection.[26] The optimum corrosion protection potential hypothesized for IGSCC of AA5083-H112 in natural sea water based on SSRT experiments was between -0.700 and -1.100 V_{SCE},[26] which is slightly more anodic than the range observed in the present results (Figure 5).

The connection between crack electrochemistry and IGSCC kinetics is based on the view that da/dt is controlled by the stress enhanced concentration of H introduced to the crack tip fracture process zone, $C_{H\sigma}$, which is supplied by the localized H concentration produced by cathodic reactions in the acidified crack tip environment.[25,36] Crack tip chemistry weakens the passive film due to low pH or chloride presence, allowing H uptake from the local solution. As crack tip overpotential for cathodic H production increases, the associated solubility of H increases and is localized by diffusion to the FPZ ahead of the crack tip surface. The $C_{H\sigma}$ accumulates within the FPZ at the region of maximum hydrostatic stress ahead of the crack tip. A variety of solutions to the crack tip diffusion problem shows that H-diffusion rate limited da/dt is related to the ratio of $C_{H\sigma}$ and the critical concentration of H necessary for damage (C_{CRIT}), as given by this relationship.[36]

$$\frac{da}{dt_{II}} = \frac{4D_{H-EFF}}{x_{CRIT}}\left[\mathrm{erf}^{-1}\left(1-\frac{C_{CRIT}}{C_{H\sigma}}\right)\right]^2 \quad (1)$$

In this formulation, $D_{H\text{-}EFF}$ is the trap-sensitive H diffusivity and x_{CRIT} is the distance ahead of the crack tip where H damage forms. Independent measurements establish $D_{H\text{-}EFF}$ for AA5083-H131.[30] Extensive results establish that x_{CRIT} is 0.9 μm for HEAC in a wide variety of alloys including AA5083-H131.[23,25] This combination of high H concentration and stress ahead of the crack tip provides the driving force for H embrittlement of the AA5083 grain boundary. Applied stress intensity, alloy flow properties and microstructure establish the local-tensile stress which inversely affects C_{CRIT}. Crack growth rate achieves

a high plateau when $C_{H\sigma}/C_{CRIT}$ is 6.25, making the squared-inverse error function term 1.0. Increasing $C_{H\sigma}/C_{CRIT}$ to 10,000 results in only a 7-fold increase in da/dt through the error function term. In sharp contrast reduced $C_{H\sigma}$ toward C_{CRIT} results in orders of magnitude reduction in da/dt. For example, the ratio of da/dt_{K15} values for applied potentials of -0.730 V_{SCE} and -1.020 V_{SCE} is 8000-to-1 from Figure 5. If $C_{H\sigma}$ equals $1000C_{CRIT}$ at -0.730 V_{SCE}, then this 8000-fold reduction in crack growth rate suggests that $C_{H\sigma}$ equals C_{CRIT} at -1.020 V_{SCE} through the leveraging of the inverse error function term in Equation 1. Crack electrochemistry developed during IGC is directly relevant to IGSCC and provides the qualitative explanation for this reduction in crack tip H concentration that controls crack growth rates at K levels above K_{TH}.

The measured applied potential dependence of IGSCC rates shown in Figure 5 confirms the proposed mechanism centered on the necessity for dissolution of β precipitates to activate sufficient near-grain boundary α corrosion that collectively leads to acidification to establish crack tip $C_{H\sigma}$. Considering the most rapid IGSCC growth rates, the applied potentials of -0.730 V_{SCE} and -0.800 V_{SCE} are each above both $E_{Br\text{-}\alpha}$ and $E_{Br\text{-}\beta}$ in acidic solutions. As in IGC, reactive dissolution of β precipitates on grain boundaries triggers dissolution of α, leading to a solution which is highly concentrated in Al^{+3} and Mg^{+2} and with an expected crack pH in the range of 2-3.[15] This acidic crack tip environment not only provides high H^+ through hydrolysis, but also destabilizes the passive film to allow H uptake into the FPZ; that is, $C_{H\sigma}$ is high and da/dt is rapid (800 nm/s to 7200 nm/s).

A severe drop in IGSCC rate occurs with bulk-polarization between -0.800 V_{SCE} and -0.900 V_{SCE}, which is close to $E_{Br\text{-}\alpha}$ (-0.870 V_{SCE})[19,20] for the acidic electrolyte expected in an actively corroding crack tip. Below $E_{Br\text{-}\alpha}$, α dissolution rate is reduced and the acidic environment is only developed to the extent possible by β dissolution, which will be more alkaline than the environment developed above $E_{Br\text{-}\alpha}$. In this crack tip environment, overpotential for H production is reduced if dominated by pH rise, less H is produced, and a more stable blocking passive film on crack tip surfaces may limit H uptake into the FPZ. The decrease in $C_{H\sigma}$ lowers crack growth rates, as indicated by the measured value (8 nm/s). The data in Figure 5 show that this severe drop in da/dt_{K15} could occur at an applied potential as low as just above -0.900 V_{SCE}, which is different from the threshold potential measured for IGC rates (-0.730 to -0.800 V_{SCE} in Figure 3). Since the crack length represented in Figure 5 (fatigue crack + IGC fissure length + some IGSCC growth) is longer than that typical of the growth rates in Figure 3, the IR drop within the IGSCC crack is expected to be larger than that in the IGC fissure, therefore IR cannot explain this potential difference. The difference must lie in the differing mechanism between IGC and IGSCC. Even though there is a lowering of corrosion rate at -0.800 V_{SCE}, the H production and uptake into the FPZ at this potential appears sufficient to cause a $C_{H\sigma}$ able to sustain HEAC.

Crack growth rate is relatively constant from -0.900 V_{SCE} to -1.020 V_{SCE}. In this range, without considering crack IR difference, the crack tip is acidified by β dissolution only, as α dissolves at a lowering rate with applied potential approaching the OCP typical of α in acidic chloride (-1.040 V_{SCE}).[19,20] The rate of IGSCC is essentially eliminated with bulk-applied potentials between -1.020 V_{SCE} and lower. This critical potential exactly aligns with $E_{Br\text{-}\beta}$ for acidic solution and is somewhat below $E_{Br\text{-}\beta}$ for neutral chloride (-0.960 V_{SCE}[31]). Below the lower limit of this potential range, both α and β dissolution are severely limited, therefore a critical crack tip chemistry is not developed and $C_{H\sigma}$ is insufficient to support da/dt. Since the lower $E_{Br\text{-}\beta}$ is the pertinent value if the crack retains some level of acidification as potential falls below about -0.900 V_{SCE}, this finding supports the proposed mechanism for IGSCC centered on the role of β dissolution in sensitized Al-Mg. If crack acidification is eliminated by cathodic polarization, then $E_{Br\text{-}\beta}$ of -0.960 V_{SCE} is the pertinent potential for very low da/dt. Since IR will likely reduce the extent of crack tip polarization to a level somewhat above the bold surface potential, it is unclear whether acid or near-neutral solution $E_{Br\text{-}\beta}$ is the pertinent value. A similar behavior is reflected by the IGC results in Figure 3, where the extent of IR-increased crack plus fissure tip potential should be equal or somewhat less that the IGSCC case in Figure 5. The key conclusion from the data in Figure 5, and this crack chemistry interpretation, is that it is certainly possible to essentially prevent IGSCC for the upper bound-susceptible S-L orientation of sensitized AA5083. The effect of crack IR does not result in an overly large amount of

applied cathodic polarization necessary to achieve this important level of protection. If potentials in the IGSCC resistant range (-1.080 V_{SCE} to -1.300 V_{SCE}) can be maintained at a fissure or crack tip with coatings or an impressed current cathodic protection system, then cathodic polarization could provide a means to minimize IGSCC in AA5083 components.

Even with excess cathodic polarization (-1.3 V_{SCE}) below $E_{Br-\beta}$, crack tip H production is either insufficient or H uptake is limited by a blocking passive film; HEAC is not clearly resolved by the data in Figure 4. In an effort to embrittle β-free AA5083 with cathodic H production, precracked as-received AA5083-H131 (DoS = 3 mg/cm^2) was stressed while highly cathodically polarized (-1.800 V_{SCE}) in NaOH,[15] which is known to promote H uptake in AA5083 based on permeation experiments.[30] Crack growth rates were within the range measured during the same experiment in air (Figure 4), illustrating the high HEAC resistance for low-DoS AA5083 stressed in this environment.[15] Additional work is required to identify the contributions to da/dt in the range of 0.1 nm to 1 nm; derived from low $C_{H\sigma}$ HEAC, creep crack growth, and plasticity-based false dcPD increase.

Collectively, the results in Figures 1 and 5, plus qualitative crack chemistry considerations, demonstrate that IGSCC in sensitized Al-Mg alloys requires β dissolution to either couple with substantial α dissolution above $E_{Br-\alpha}$ to produce extreme acidification and H uptake, or to produce some acidification at lower potentials where α dissolution is limited. Without the acidic environments developed by β + α and by β-only dissolution, H uptake and $C_{H\sigma}$ are not sufficient to support a measurable da/dt. This explanation is being further tested by experiments with β-free AA5083-H131 (DoS of 3 mg/cm^2) stressed in a bulk electrolyte which simulates the low pH acidic solution created by interactive Al^{+3} and Mg^{+2} cation hydrolysis.[15] Rapid crack growth rates were measured, on the order of 50 nm/s and substantially higher than the very low da/dt_{K15} typical of the as-received AA5083 stressed in near-neutral NaCl solution (1.5 nm/s).[12] The rates measured for IGSCC in simulated crack solution correlate with the predictions of Equation 1, characteristic of H diffusion rate limited crack growth.[23] These results confirm the requirement of an acidic-occluded crack environment for H production and uptake, as necessary for H embrittlement of Al-Mg alloys.

Modeling potential controlled IGSCC

The coupled environmental fracture model (CEFM), developed for film rupture-based IGSCC in sensitized stainless steel[37] and amplified to center on crack growth due to interactive crack tip dissolution, film rupture and H damage,[38] was recently applied to predict the effect of bold-surface electrochemical potential on IGSCC in Al-Mg.[35] The CEFM model couples bold-surface net-cathodic currents with the net-positive current flowing through the crack mouth and originated by dissolution after crack tip passive film rupture, which is local strain rate and hence K sensitive.[39] Crack tip hydrogen production is qualitatively linked to crack tip dissolution which favors acidification and IR difference.[35,37] Lacking a specific crack tip fracture criterion and associated distance, the CEFM crack growth rate is equated to the product of microfracture event dimension squared and event frequency normalized by crack front length (e.g., SENT thickness). Threshold K_{TH} is interpreted as the K level below which film rupture does not occur and the crack current tends to a very low value. This approach aligns with the hypothesized mechanism for IGSCC in sensitized Al-Mg;[7,12,23,24] specifically, crack tip corrosion leads to acidification which couples with IR-lowered crack tip potential to enhance H production and uptake key to HEAC.

The CEFM requires calibration with known crack growth rate data for a specific environmental condition, which was accomplished for the near-neutral 0.6 M NaCl environment using da/dt measurements reported for a resistant crack orientation in AA5083-H321 with a lightly sensitized (DoS of 7 mg/cm^2) equiaxed grain structure.[7,35] For this condition, the CEFM predicted the beneficial effect of decreasing bold surface potential on da/dt; specifically, da/dt at high K (25 MPa$\sqrt{m}$) declined from 3 nm/s at -0.540 V_{SCE} to 0.1 nm/s at -0.800 V_{SCE} and lower.[35] The rate of IGSCC was predicted to equal 0 below this potential, with the 0.1 nm/s growth rate modeled as due to creep crack growth apart from H embrittlement. This predicted trend qualitatively parallels the results for AA5083-H131 shown in Figures 1, 4 and 5. However, the CEFM predictions for IGSCC rate in AA5083 are specific to crack tip passive

dissolution reaction of Al, without corrosion current due to reactive β and α dissolution above $E_{Br-\beta}$ and $E_{Br-\alpha}$.[35] As such, this calibration of the CEFM predictions is not relevant to the present investigation of IGSCC in sensitized AA5083-H131. At best for sensitized Al-Mg, mechanical rupture of a likely passivated Al surface in the potential range of -0.900 V_{SCE} and lower (Figure 5), could be modeled by the CEFM approach.

Substantial uncertainties are associated with application of the CEFM to predict rates of IGSCC by HEAC in sensitized Al-Mg alloys. Clearly, K_{TH} and da/dt versus K are fundamentally based on the concentration of H trapped at highly stressed sites within the crack tip FPZ.[36] The challenge is to predict this concentration and relate it through a physically based failure criterion to predict K_{TH} or da/dt versus K. The CEFM provides one approach to modeling crack electrochemistry and H production, but controversy exists.[40–42] No evidence was presented that validates the capability of the CEFM to predict crack tip anodic current density, overpotential for H production, and H uptake in an actively dissolving α grain boundary with discontinuously arrayed reactive β precipitates. As a second concern, the present analysis and CEFM approach each center on crack tip H embrittlement; however, there are important differences. For CEFM, the microfracture event frequency was modeled as the ratio of crack tip strain rate to passive film fracture strain;[35] both quantities are uncertain in spite of decades of research. Alternately, microfracture frequency is extracted from analysis of the noise transients associated with the measured coupling current,[38] but these measurements were not reported for AA5083.[35] The microscale crack advance distance for AA5083 was apparently calibrated from a measured da/dt to equal 57.8 μm, using an event frequency from crack tip strain rate given as a function of K following analysis by Shoji.[43] Predicted microfracture dimensions for other da/dt (and K) levels were between 2000 μm (K = 12 MPa√m) and 45 μm (K = 30-45 MPa√m); for Stage II K levels, this distance was sensibly constant at 40-60 μm.[35] This fracture length was similarly predicted to equal 49 μm for an ultra-high strength martensitic steel subjected to HEAC in NaOH solution.[35,38] These distances were ascribed to the location of crack tip hydrostatic stress controlled H damage sites, and were also associated with a microstructure characteristic such as precipitate spacing or grain size,[38] and/or H diffusion distance.[35] Crack tip H diffusion and mechanics analyses were not reported, and the reason for a microstructure-based critical distance was not put forth.

These CEFM-based microscale distances for discontinuous H crack advance are 40 to 500 times larger than the x_{CRIT} of 1 μm (Equation 1), which was established by analysis of HEAC growth rate and threshold stress intensity data for a wide range of high strength alloys, coupled with considerations of various solutions to the crack tip H diffusion problem.[25,36] Stated alternately, HEAC in a wide variety of alloys progresses at rates that cannot be sustained by H diffusion over a distance of order 50-100 μm based on measured trap sensitive H diffusivities. However, the CEFM formulation implicitly assumes that such H diffusion occurs and moreover does not limit da/dt relative to the frequency of crack tip film rupture.[35] A distance of order 1 μm is consistent with modern predictions of the location of the maximum crack tip hydrostatic tension, ahead of a either a blunted[44] or sharp-shielded crack tip.[45] A classic upper bound of this distance is provided by $K^2/\sigma_{YS}E$, which is 10 μm for the flow properties of AA5083 and 0.7 μm for a high strength steel such as 4340 (σ_{YS} = 1600 MPa), each stressed at K of 15 MPa√m. While this upper bound is 100 μm for AA5083 loaded to K of 45 MPa√m, this high K is not physically realistic and microscale stress concentration associated with β and strain gradient plasticity are likely to substantially reduce this value toward 1 μm, as affirmed for other Al alloys.[25] Interaction of H with trap sites in the corroding α-β microstructure must also be considered with regard to the critical distance,[23] but this geometry does not change the conclusion that x_{CRIT} (Equation 1) for IGSCC/HEAC in sensitized AA5083 is 1 μm or smaller dictated by the grain boundary β spacing of 300 nm.[46] A critical distance, in the range of 100 nm to 1 μm, is likely to be similar for sensitized Al-Mg alloys with discontinuous β precipitation on grain boundaries. The very large microfracture distances predicted by the CEFM (for example 2,000 μm at K of 12 MPa√m[35]) are particularly unreasonable. The large microfracture dimension in the CEFM formulation may be associated with selection of the larger and less frequent current transients for the steel case,[38] and with the assumed crack tip strain rate versus K dependence when coupling current

noise is not measured.[35] As the microfracture frequency increases, the crack advance distance falls, with the limiting case being near-continuous HEAC and a very short microfracture distance.

IGSCC in sensitized Al-Mg alloys is reasonably explained by a coupled crack tip α-β dissolution plus H embrittlement mechanism. The crack tip mechanics framework exists to predict K_{TH} and da/dt versus bold-surface electrochemical potential. However, challenges remain in quantifying occluded-crack electrochemistry and the associated concentration of H produced in the crack tip FPZ, as well as a fundamental association of such trapped H with cracking properties.

CONCLUSIONS

Intergranular stress corrosion cracking (IGSCC) in sensitized AA5083-H131 requires crack tip Al-Mg matrix and β (Al_2Mg_3) precipitate dissolution to produce a local-acidic environment that yields a high over-potential for H production and uptake leading to H embrittlement controlled crack growth. When β dissolution is mitigated by either low DoS or by bulk cathodic polarization, IGSCC (and IGC) are nearly eliminated during slow rising K (and static-low stress intensity) loading for exposure in neutral NaCl solution. Specific conclusions are as follows.

- Intergranular "crevice" corrosion from a fatigue precrack is measured as a precursor to IGSCC and explained based on occluded-crack/fissure chemistry changes in response to varying external polarization.
- Intergranular corrosion is nearly eliminated for a bold-surface potential between -0.975 V_{SCE} and -1.300 V_{SCE}, but remains finite likely due to cathodic corrosion.
- For the highly susceptible S-L crack orientation, IGSCC rates are nearly eliminated by applied cathodic polarization below -1.020 V_{SCE}, which puts the crack tip below both the pH-sensitive Al-Mg matrix and β breakdown potentials.
- Both IGC and IGSCC are accelerated with bulk-applied anodic potentials greater than -0.800 V_{SCE}.
- A crack tip mechanics model based on H diffusion limitation of IGSCC growth rate exists to couple with accurate determination of crack tip fracture process zone H concentration, and suggests a sub-micrometer critical distance.
- Controlling β dissolution by cathodic polarization may provide a means to manage IGSCC.

ACKNOWLEDGEMENTS

This research was sponsored by the Office of Naval Research, under Grant N000140810315 with Dr. Airan Perez as the Scientific Officer. Professors Robert G. Kelly and John R. Scully provided important inputs on crack electrochemistry and IGC kinetics. Aluminum alloy 5083-H131 was provided by the Alcoa Technical Center and Francine Bovard. These contributions are gratefully acknowledged.

REFERENCES

1. J.L. Searles, P.I. Gouma, R.G. Buchheit, "Stress Corrosion Cracking of Sensitized AA5083," *Metall. Mater. Trans. A.* 32 (2001): p. 2859.
2. R. Goswami, G. Spanos, P.S. Pao, R.L. Holtz, "Microstructural Evolution and Stress Corrosion Cracking Behavior of Al-5083," *Metall. Mater. Trans. A.* 42 (2011): p. 348.
3. R. Goswami, R.L. Holtz, "Transmission Electron Microscopic Investigations of Grain Boundary Beta Phase Precipitation in Al 5083 Aged at 373 K (100 °C)," *Metall. Mater. Trans. A.* 44 (2013): p. 1279.
4. G. Scamans, "Low Temperature Sensitisation of AA5xxx Alloys," Innoval, IR07-197, January, 2008.

5. E.H.J. Dix, A. Anderson, M.B. Shumaker, “Influence of Service Temperature on the Resistance of Wrought Aluminum-Magnesium Alloys to Corrosion,” *Corrosion* 15 (1959): p. 55.
6. Y. Zhu, D.A. Cullen, S. Kar, M.L. Free, L.F. Allard, “Evaluation of Al_3Mg_2 Precipitates and Mn-Rich Phase in Aluminum-Magnesium Alloy Based on Scanning Transmission Electron Microscopy Imaging,” *Metall. Mater. Trans. A.* 43 (2012): p. 4933.
7. R.H. Jones, D.R. Baer, M. Danielson, J.S. Vetrano, “Role of Mg in the Stress Corrosion Cracking of an Al-Mg Alloy,” *Metall. Mater. Trans. A.* 32 (2001): p. 1699.
8. J. Gao, D.J. Quesnel, “Enhancement of the Stress Corrosion Sensitivity of AA5083 by Heat Treatment” *Metall. Mater. Trans. A.* 42 (2010): p. 356.
9. F.S. Bovard, “Sensitization and Environmental Cracking of 5xxx Aluminum Marine Sheet and Plate Alloys,” in Corrosion in Marine and Saltwater Environments II, eds. D.A. Shifler, T. Tsuru, P.M. Natishan, S. Ito (Pennington, NJ: ECS, 2003), p. 477.
10. R.L. Holtz, P.S. Pao, R.A. Bayles, T. Longazel, R. Goswami, “Corrosion Fatigue and Stress Corrosion Cracking of Sensitized Al-Mg Structural Alloys,” Symposium on Structural Materials for Aerospace and Defense (Columbus, OH: MS&T; 2011).
11. C.B. Crane, R.P. Gangloff, “Stress Corrosion Cracking of Low Temperature Sensitized AA508,” DoD Corrosion Conference 2011 (Houston, TX: NACE, 2011), www.corrdefense.org.
12. C.B. Crane, R.P. Gangloff, “Stress Corrosion Cracking of Sensitized 5083-H131,” to be submitted to: *Metall. Mater. Trans. A*, 2013.
13. D. Mizuno, R.G. Kelly, “Galvanically Induced Intergranular Corrosion of AA5083-H131 Under Atmospheric Exposure Conditions: Part 1- Experimental Characterization,” *Corrosion* 69 (2013): p. 580.
14. ASTM G67-04, “Standard Test Method for Determining the Susceptibility to Intergranular Corrosion of 5xxx Series Aluminum Alloys by Mass Loss After Exposure to Nitric Acid (NAMLT test)” (West Conshohocken, PA: ASTM), 2013.
15. C.B. Crane, R.G. Kelly, R.P. Gangloff, “Crack Tip Chemistry Control of Intergranular SCC in Al-Mg Alloys,” to be submitted to *Corrosion,* 2013.
16. M.L. Lim, J.C. Scully, R.G. Kelly, “Studies of Intergranular Corrosion Penetration as a Function of Electrochemical and Metallurgical Conditions,” DoD Corrosion Conference 2011 (Houston, TX: NACE, 2011), www.corrdefense.org.
17. S. Jain, M.L.C. Lim, J.L. Hudson, J.R. Scully, “Spreading of Intergranular Corrosion on the Surface of Sensitized Al-4.4Mg Alloys: A General Finding,” *Corros. Sci.* 59 (2012): p. 36.
18. M.L. Lim, J.C. Scully, R.G. Kelly, “Intergranular Corrosion Penetration in AA5083 as a Function of Electrochemical and Metallurgical Conditions,” *Corrosion* 69 (2013): p. 35.
19. E. Bumiller, R.G. Kelly, “Intergranular Corrosion in AA5xxx: A Case for Continuous Attack with a Discontinuous Active Path” DoD Corrosion Conference 2011 (Houston, TX: NACE, 2011), www.corrdefense.org.
20. E. Bumiller, “Intergranular Corrosion in AA5XXX Aluminum Alloys with Discontinuous Precipitation at the Grain Boundaries” (PhD Dissertation, University of Virginia, 2011), p. 218.
21. D. Mizuno, R.G. Kelly, “Galvanic Corrosion Behavior of AA5083-H131 in Contact with 4340 Steel Under Atmospheric Exposure Conditions,” DoD Corrosion Conference 2011 (Houston, TX: NACE, 2011), www.corrdefense.org.
22. M.L. Lim, J.C. Scully, R.G. Kelly, University of Virginia, correspondence to authors, 2012.
23. C.B. Crane, R.P. Gangloff, “Dissolution and Hydrogen Diffusion Control of IGSCC in Sensitized Al-Mg Alloys,” in *Hydrogen Effects on Materials*, eds. B.P. Somerday, P. Sofronis (New York, NY: ASME, 2013), in press.
24. D. Tanguy, B. Bayle, R. Dif, T. Magnin, “Hydrogen effects During IGSCC of Pure Al–5Mg Alloy in NaCl Media,” *Corros. Sci.* 44 (2002): p. 1163.
25. R.P. Gangloff, “Diffusion Control of Hydrogen Environment Embrittlement in High Strength Alloys” in *Hydrogen Effects on Material Behavior and Corrosion Deformation Interactions*, eds N.R. Moody, A.W. Thompson, R.E. Ricker, G.W. Was, R.H. Jones (Warrendale, PA: The Minerals, Metals & Materials Society, 2003), p. 477.
26. M.-S. Han, “Optimization of Corrosion Protection Potential for Stress Corrosion Cracking and Hydrogen Embrittlement of 5083-H112 Alloy in Seawater,” *Met. Mater. Int.* 14 (2008): p.203.

27. F.S. Bovard, Alcoa Technical Center, correspondence to authors, 2012.
28. R.P. Gangloff, D.C. Slavik, R.P. Piascik, R.H. Van Stone, “Direct Current Electrical Potential Measurement of the Growth of Small Cracks,” in *Small Crack Test Methods, ASTM STP 1149*, eds. J. Larsen, J. Allison (Philadelphia, PA: ASTM, 1992), p. 116.
29. J.K. Donald, J. Ruschau, “Direct Current Potential Difference Fatigue Crack Measurement Techniques,” in *Fatigue Crack Measurement: Techniques and Applications*, eds. K. Marsh, R. Smith, R. Ritchie (West Midlands, UK: EMAS, 1991), p.11.
30. J. Ai, M.L. Lim, J.R. Scully, “Hydrogen Permeation Behavior in an Al-Mg Alloy (AA 5083) as a Function of Degree of Sensitization and Orientation,” *Corrosion*, in review, 2013.
31. N. Birbilis, R.G. Buchheit, “Electrochemical Characteristics of Intermetallic Phases in Aluminum Alloys,” *J. Electrochem. Soc.*152 (2005): p. 140.
32. E. Brillas, P.L. Cabot, F. Centellas, J.A. Garrido, E. Pe, R. M. Rodroa, “Electrochemical Oxidation of High-Purity and Homogeneous Al-Mg Alloys with Low Mg Contents,” *Electrochim. Acta* 43 (1998): p. 799.
33. T. Takemoto, I. Okamoto, “Stress Corrosion Cracking and Anodic Dissolution Behavior of 5083 Aluminum Alloy,” *Trans. JWRI* 13 (1984): p.285.
34. M. Elboujdaini, M.T. Shehata, E. Ghali, “Stress Corrosion Cracking and Corrosion Fatigue of 5083 and 6061 Aluminum Alloys,” *Microstruct. Sci.* 25 (1997): p.41.
35. S.-K. Lee, P. Lv, D.D. Macdonald, “Customization of the CEFM for Predicting Stress Corrosion Cracking in Lightly Sensitized Al–Mg Alloys in Marine Applications,” *J. Solid State Electrochem* (2013) DOI: 10.1007/s10008-013-2111-6.
36. R.P. Gangloff. “Hydrogen Assisted Cracking of High Strength Alloys,” in: *Comprehensive Structural Integrity*, eds. I. Milne, R.O. Ritchie, B. Karihaloo, J. Scott, P. Petit (New York, NY: Elsevier Science, 2003), p. 31.
37. D.D. Macdonald and M. Urquidi-Macdonald, “A coupled Environment Model for Stress Corrosion Cracking in Sensitized Type 304 Stainless Steel in LWR Environments” *Corros. Sci.* 32 (1991): p. 51.
38. S. Lui and D.D. Macdonald, “Fracture of AISI 4340 Steel in Concentrated Sodium Hydroxide Solution”, *Corrosion* 58 (2002): p. 835.
39. F.P. Ford, “The Crack-Tip System and Its Relevance to the Prediction of Cracking in Aqueous Environments,” in *Environment-Induced Cracking of Metals*, eds. R. P. Gangloff and M. B. Ives (Houston, TX: NACE, 1990), p. 139.
40. P.L. Andresen, “Discussion on ‘Determination of the Fate of the Current in the SCC of Sensitized Type 304 SS in High Temperature Aqueous Systems,’” *Corros. Sci* 37 (1995): p. 2087.
41. P.L. Andresen, F.P. Ford, “Response to ‘On the Modeling of Stress Corrosion Cracking of Iron and Nickel Base Alloys in High Temperature Aqueous Environments,’” *Corros. Sci.* 38 (1996): p. 1011.
42. D.D. Macdonald, “Clarification of Issues Raised by P.L. Andresen and F.P. Ford in Their Response to “On the Modeling of Stress Corrosion Cracking of Iron and Nickel Base Alloys in High Temperature Aqueous Environments.” *Corros. Sci*. 39 (1997): p. 1487.
43. T. Shoji, Z. Lu, H. Murakami, “Formulating Stress Corrosion Cracking Growth Rates by Combination of Crack Tip Mechanics and Crack Tip Oxidation Kinetics,” *Corros. Sci*. 52 (2010): p. 769.
44. R.M. McMeeking, “Finite Deformation Analysis of Crack-Tip Opening in Elastic-Plastic Materials and Implications for Fracture,” *J. Mech. Phys. Solids*, 25 (1977): p. 357.
45. U. Komaragiri, S.R. Agnew, R.P. Gangloff and M.R. Begley, “The Role of Macroscopic Hardening and Individual Length Scales on Crack Tip Stress Elevation from Phenomenological Strain Gradient Plasticity”, *Journal of Mechanics and Physics of Solids*, 56 (2008): p. 3527.
46. N. Birbilis, M.L. Lim, A.K. Gupta, C.H.J. Davies, S.P. Lynch, R.G. Kelly, J.R. Scully, “Quantification of Sensitization in AA5083-H131 via Imaging Ga Embrittled Fracture Surfaces,” *Corrosion* 69 (2013): p. 396.